Author Manuscript
Accepted for publication in a peer-reviewed journal

NIST National Institute of Standards and Technology • U.S. Department of Commerce

Published in final edited form as:
Polym Degrad Stab. 2018 ; 154: . doi:10.1016/j.polymdegradstab.2018.05.030.

Oxidation Reactions in Kink Banded Regions of UHMMPE Fiber-Based Laminates Used in Body Armor: A Mechanistic Study

Zois Tsinas[a], **Amanda L. Forster**[b,*], and **Mohamad Al-Sheikhly**[a,*]

[a]Materials Science and Engineering Department of University of Maryland, College Park, MD, USA

[b]Material Measurement Laboratory, National Institute of Standards and Technology, Gaithersburg, MD, USA

Abstract

This work demonstrates the synergy between the thermo-mechanical and humidity induced degradation as well as the oxidation reactions in the kink-banded areas of ultra-high molar mass polyethylene (UHMMPE) fiber-based laminates used in body armor. For aged materials, the energy-dispersive X-ray spectroscopy (EDS) and Fourier transform infrared spectroscopy (FTIR) results reveal high concentrations of oxygen containing products, and the EPR results demonstrate the presence of the peroxyl radicals ($RO_2^{\bullet}$) in the kink-banded areas. After one year of dark ambient storage, very long-lived $RO_2^{\bullet}$ radicals were observed primarily in the samples exposed to ageing conditions of elevated temperatures, humidity, and mechanical stress. The total percentage of crystallinity, as measured by differential scanning calorimetry, of the kinkbanded fibers was unchanged, indicating that the degradation occurs primarily in the amorphous region, and may also involve recrystallization processes of the degraded chains. However, the most abundant orthorhombic crystalline phase decreases from 77 % to 70 %. This decrease in the orthorhombic structure leads to more diffusion of oxygen into the kink-banded region, enhancing the oxidation processes. No changes are observed in the monoclinic phase of the kinked fibers, which remained constant and constituted ~2 % of the total crystallinity.

Keywords

UHMMPE fibers; kink bands; body armor; free radicals; oxidation; degradation

1. Introduction

Modern body armors are commonly designed using flexible, ballistic-resistant fabrics made from high strength polymers such as ultra-high molar mass polyethylene (UHMMPE). This polymer can be processed via gel spinning into fibers with high tensile strength-to-weight ratios and superior fatigue, corrosion, and chemical resistance as compared to other polymeric materials [1–5]. Polyethylene (PE) can exist as low-density polyethylene (LDPE), high-density polyethylene (HDPE) and UHMMPE. HDPE and UHMMPE can have the

*Corresponding authors.

same density, but the molar mass of UHMMPE is much higher. In general, the crystals in polyethylene orient in structures known as crystalline folded lamella (lamellar orthorhombic crystal phase) with a typical thickness of 10 – 50 nm and length of 10 – 50 μm [6]. The lamellae are separated by amorphous regions that are approximately 50 nm in length [7]. A single PE chain can exist in the amorphous phase as well as orient in many crystalline lamellae separated by tie molecules [8]. UHMMPE fibers are used in body armor applications. These fibers have different properties as compared to bulk PE because of the orientation process used in their manufacture. The fibers are extended 50 to 100 times their original length during a process known as “super-drawing” [9, 10]. UHMMPE fibers are also highly crystalline, with a total crystallinity of approximately 85%. The drawing process converts the folded lamellar orthorhombic found in bulk HDPE into extended orthorhombic lamellar crystals [11, 12]. Overall, highly oriented UHMMPE fibers are generally believed to contain four morphological phases: a rigid extended orthorhombic phase, a monoclinic phase, an amorphous phase and an intermediate phase also known as oriented crystal-amorphous transition area with low molecular mobility [13, 14]. The amorphous phase in this material is characterized by high mobility due to chain ends, defects, and nano-voids [14].

Degradation of UHMMPE fibers under normal use conditions is a combined effect of mechanical stress, elevated temperatures, and humidity that are controlled by several factors such as the crystallinity of the polymer, the presence of oxygen and other impurities in the material, the concentration and type of antioxidant, and the formation of free radicals in the polymer backbone [15–17]. The application of mechanical stress in these highly crystalline and oriented fibers can lead to morphological deformations known as kink bands [18]. Kink bands appear as a series of successive bands at an angle of 50° to 60° to the fiber axis [18]. These bands form where the orientation of the polymer chains suddenly changes and are manifested as a narrow triangular or wedged-shaped area on the fiber. Edmunds proposes a model for the kink band formation in highly oriented aramid fibers [19]. In this model, kink bands are assumed to be made from straight limbs and sharp corners, based on previous work by Hunt et al. [20]. The formation of such defects along the axis of the fibers is mainly due to compressive and shearing forces, and the lack of strong lateral support between the highly oriented polymer chains. As compressive forces and the shearing between the polymer chains in the fibers increase, deformation increases and begins to propagate from the surface to the fiber axis (fibers in this study are approximately 25 μm in diameter). With additional compressive and shearing deformation, more polymer chains slip past each other, more fibrils [21] are misaligned from the fiber axis, and the micro-buckled regions get larger. As a result, new kinks begin to form along the fiber axis. Ultimately, the fiber will fracture under tension to form a kink band break [18, 22, 23]. The process of a kink band break, also known as knuckle formation, is not reversible and voids are formed within the kink band as a result of lateral splitting between the polymer chains [24]. Although the formation of kink bands in high strength polymer fibers used in body armor applications has been previously reported and characterized in the case of poly(*p*-phenylene terephalamide) PPTA and poly(*p*-phenylene benzobisoxazole) PBO fibers [18, 22–24], their role in the long-term stability and failure of UHMMPE fibers is not fully identified. Notable exceptions are the recent work of Attwood et al. who studied the compressive strength of commercially

available UHMMPE fibers and the out-of-plane compressive response of these fibers and their composites [25, 26]. Additionally, the formation of kink bands upon compression of commercially available UHMMPE fibers was also observed by Liu et al. in his study on composite beams made by a leading market company [27]. A more recent work by Hazzard et al. on thin composite laminates showed that UHMMPE fibers in the laminate develop kink bands upon low velocity impact, which further supports the previous findings relating the formation of kink bands with compressive forces [28]. According to Fleck and his review on the compressive failure of UHMMPE fiber composites, the compressive strength of long fiber composites is a complex mechanism governed by elastic and plastic micro-buckling, fiber crushing and fiber splitting phenomena, as well as buckle delamination and shear band formation at a 45° angle to the fiber axis [29].

In addition to mechanical stress (tensile and compressive stresses), temperature plays an important role in the stability of polyolefins such as UHMMPE. UHMMPE fibers used in body armor are not exposed to the extreme temperatures that can result in bond scissions and depolymerization, since the maximum temperature observed during use or storage is approximately 67 °C [30]. However, when strain is applied and temperature approaches the range of the α-relaxation temperature (80 °C) [31], polymer chains will tend to increase their entropy by folding back on themselves [32]. Rotational motion of the C-C bonds in the backbone of the UHMMPE chains can occur more easily, thus increasing the free volume of the chains and making them more mobile [32]. Chain slippage only dominates at temperatures near the alpha relaxation, therefore bond rupture is the expected degradation mechanism during use and storage of body armor [15].

Mechanically and thermally induced bond scissions in the backbone of UHMMPE, and the formation of carbon centered free radicals, have a significant role in the oxidative degradation of the material. Oxygen can be both initially present in the fibers as well as diffuse into the polymer over time [33]. During industrial processing of the UHMMPE fibers, oxygen can become entrapped in the structure and it is practically impossible to prepare a totally oxygen-free polymer, even in the presence of an inert gas [34, 35]. Furthermore, the solubility and diffusion of oxygen into the fibers further complicates the kinetics of the oxidation reactions. The oxygen solubility and diffusivity are functions of temperature [36]. In general, the solubility decreases slightly with decreasing temperature, while the diffusivity increases [36]. In the case of highly oriented UHMMPE fibers, oxygen transport takes place almost exclusively through the amorphous regions of the polymer and the crystalline regions provide barriers to impede oxygen flow [37]. The extent of these barriers, and their influence on the diffusion of oxygen through the amorphous regions of the polymer, depends on the molecular orientation of the polymer chains and their packing density in the highly drawn fibers [37]. However, the presence of kink bands will allow oxygen to diffuse more easily into the fibers through the voids created by the lateral splitting of the polymer chains, leading to higher local oxygen concentrations at the kink bands. In the presence of oxygen solubilized in the amorphous phase and kink bands of UHMMPE, alkyl free radicals will become involved in a series of reactions that can further decrease the molar mass of the polymer and result in products such as ketones, carboxylic acids, alcohols and esters [15, 38, 39]. These moieties give the polymer more hydrophilic properties,

rendering it more susceptible to attack by water, which can in turn penetrate into the polymer and induce more oxidation over time [15].

Previous studies have focused on understanding how compressive stress leads to the formation of kink bands into the UHMMPE fibers through complex micro-buckling phenomena. However, the nature of the changes that the fibers undergo due to the formation of these kink bands are not yet very well understood. Such defects can have a major impact on the polymer chain orientation, the crystallinity, and the chemistry of the polyethylene, which can adversely affect the long-term stability of the material. Overall, the goal of this study is to investigate the physical and chemical changes induced in UHMMPE fibers by the formation of the kink bands and their effect on the long-term stability of the material.

2. Experimental

2.1. Sample description

The ballistic resistant armor panels used in this study are commercial products and were manufactured from highly-crystalline UHMMPE fibers combined with an elastic resin material to form a non-woven unidirectional tape. The UHMMPE fibers are described by the manufacturer as having a molar mass between 3 and 5 million amu, and contain a hindered phenolic antioxidant [16]. Two layers of the unidirectional tape are laminated together in a crisscross pattern, where each layer is placed at a 90° angle from the layer above and below to form a laminate. A thin film of low density polyethylene (LDPE) is added on both sides of each laminate, with a thickness of 0.35 mm, to prevent adjacent laminates from sticking together when they are layered on top of each other in the soft body armor [40, 41]. A representative UHMMPE-based material used in body armor applications usually consists of 80 % UHMMPE fibers, 13 % resin, and 7 % LDPE by mas [41, 42]. In this study, the body armor used was comprised of 27 laminates. The armor was stored in dark ambient conditions prior to and after having been subjected to an accelerated ageing condition. In this work, the armor panels were aged according to the protocol described in NIJ Standard 0101.06. The panels were placed into specially designed chambers at 65 °C, 80 % relative humidity, and subjected to 0.52 rad/s tumbling for 72,000 total rotations, or approximately 240 h. A series of temperature/relative humidity data loggers were used to monitor the consistency of the chamber conditions during the exposure time. In addition to this protocol, a folding protocol was developed and used in this study to allow for the evaluation of the isolated effect of mechanical stress on the UHMMPE fibers when part of the laminated structure is folded. Laminates removed from a new armor panel were folded once and constrained in half (180° fold), and then placed in into an oven at 80 °C, under ambient pressure and humidity conditions for a period of 336 h. A thermocouple was used to monitor the consistency of the oven temperature during the exposure time.

2.2. Extraction of UHMMPE Fibers

The UHMMPE fibers used in this study were extracted from laminates that were incorporated in body armor. Pieces of the laminates were cut and immersed in beakers containing chloroform. Mild agitation by hand was performed periodically, until the laminates were visually observed to separate. Then the samples were left overnight into the

chloroform solution to allow for the binder resin to fully dissolve in the chloroform. The UHMMPE fibers and the LDPE film do not dissolve in chloroform and precipitate from solution. Filtration was performed to separate the UHMMPE fibers and LDPE film from the chloroform solution containing the binder resin. Next, to eliminate any residual traces of resin from the surface of UHMMPE fibers, the fibers were transferred back to the beaker and more chloroform was added and left overnight. This process was repeated two more times for a total of 4 days. The UHMMPE fibers were air dried and stored under desiccation until testing.

2.3. Fiber topography and chemical composition

The shape and the surface morphology of the UHMMPE were characterized by scanning electron microscopy (SEM) using a Hitachi.[1] S-2400 variable pressure SEM equipped with an Xray detector that allows for elemental analysis through energy dispersive spectroscopy (EDS). The fibers were evenly spread over slabs and left under vacuum overnight to eliminate any traces of humidity and oxygen bound to the surface of the fibers prior to analysis. The analysis was conducted using variable pressure mode at 15 keV.

2.4. Oxidation measurement

Oxidation of UHMMPE fiber samples and binder resin material was measured using Fourier Transform Infrared Spectroscopy (FTIR). A Thermo Nicolet NEXUS 670 FTIR equipped with an attenuated total reflectance (ATR) accessory was used to measure the oxidation of the materials. The final spectrum of each sample represents the average of 128 individual scans with a resolution of 2 cm^{-1} between 650 cm^{-1} and 4000 cm^{-1} wavenumbers. A background was collected and subtracted prior to each sample run. Three replicates were prepared for each sample. Spectra analysis, including baseline correction and normalization, was performed. The spectra were baseline corrected and normalized using the peak at 1472 cm^{-1}, which was attributed to the CH bending [43, 44]. Typical standard uncertainties for spectral measurement are 2 cm^{-1} in wavenumber and 5 % in peak intensity. To evaluate the degree of oxidation, the overlapping peaks between 1712 cm^{-1} and 1735 cm^{-1}, assigned to the oxidation products (ester and ketone groups), were deconvolved using commercial software.

2.5. Free radical identification

Electron Paramagnetic Resonance (EPR) spectroscopy was used to identify the structure of the free radicals in the kink banded areas. The measurements were carried out at room temperature in the presence of oxygen approximately two months after removing the body armor samples from the ageing chamber and after extracting the fibers from the laminate. The EPR spectra were acquired on a ESP300 spectrometer (Bruker Biospin, Billerica, MA) using the following instrument parameters: microwave frequency of 9.435 GHz, microwave power of 6.346 mW, frequency modulation of 100 kHz, modulation amplitude of 6.23 G,

[1]The full description of the procedures used in this paper requires the identification of certain commercial products and their suppliers. The inclusion of such information should in no way be construed as indicating that such products or suppliers are endorsed by NIST or are recommended by NIST or that they are necessarily the best materials, instruments, software or suppliers for the purposes described.

receiver gain of 56,400, center field at 3350 G, a sweep width of 800 G, a conversion time of 40.96 ms, and a time constant of 20.48 ms. The instrument was calibrated prior to the measurements using a 2,2diphenyl-1-picrylhydrazyl (DPPH) stable free-radical control sample.

2.6. Identification of the changes in the crystal structure

Differential scanning calorimetry was carried out using a TA Q2000 differential scanning calorimeter (DSC) (TA Instruments). UHMMPE fibers extracted from new and aged panels were coiled around a wire and placed at the bottom of aluminum hermetic pans. The typical weight of the samples was kept between 3 mg and 5 mg to increase resolution. Samples were held at 25 °C for 5 min and then heated to 180 °C at a rate of 10 °C/min. The measurements were conducted under flowing nitrogen at a flow rate of 25 mL/min. The melting curves of the crystals were deconvolved into 4 peaks, which were assigned to the melting of different crystal phases. The melting points were characterized by the temperature of the peak maximum, and the area under each peak was integrated to assess the crystal composition of the material. Additionally, wide angle X-ray scattering (WAXS) measurements were conducted using a Xenocs Xeuss SAXS/WAXS small angle X-ray scattering system. The instrument was equipped with an x-ray video-rate imager for SAXS analysis with a minimum Q = 0.0045 $Å^{-1}$, detector separate x-ray video-rate imager for WAXS analysis (up to about 45° 2θ), and a Linkam stage for controlling the temperature of the sample from about -100 °C to 250 °C. The incident beam, diffracted beam and sample chamber were kept under vacuum. The fibers were mounted across a small groove formed by a copper block used along with the heating stage to acquire data at various temperatures. The bundle of fibers was mounted horizontally, perpendicular to the direction of the X-ray beam. In these experiments, silver behenate was used as a control and each sample and condition was tested in duplicate.

3. Results and discussion

3.1. Kink Band Formation

Fibers from aged and unaged armors were examined for evidence of kink bands using SEM. The images in Fig. 1. illustrate the mechanical compressive and tensile stress-induced formation of the kink bands in the fibers during folding of the armor panels. As shown in Fig. 1, the kink bands are absent in the UHMMPE fibers extracted from unaged body armor and at areas away from the bending site in armors that were aged using the folding protocol (Fig. 1(d)). However, the formation of kink bands can clearly be seen in Fig. 1(b), fibers extracted from aged (NIJ protocol) vests. The kink bands are uniformly spread across the fibers of all the samples exposed to the NIJ protocol. As expected, fibers extracted from laminates of the armor that were folded at an 180° angle (folding protocol) revealed severe kink band and knuckle formation at the bending point, as shown in Fig. 1(c). These results clearly demonstrate that mechanical stress is the primary mechanism of kink band formation in UHMMPE fibers

3.2 The relatively high concentration of oxidative products at the kink bands

SEM-EDS was used to determine the relative oxygen concentrations in the kink band areas as compared to other areas along the fiber. The relative oxygen concentrations were measured in the fibers extracted from unaged body armor, armor aged with the NIJ protocol, and aged armor with the folding protocol. The areas on these fibers that were analyzed via SEM-EDS to evaluate the oxygen concentrations were the following: a) random areas on fibers extracted from unaged vests, referred to as “New/No Kink-Bands”; b) areas without kink bands conditioned via the NIJ protocol, referred to as “NIJ/No Kink-Bands”; c) areas without kink bands on fibers exposed to the folding protocol, referred to as “Folding/No Kink-Bands”; d) areas with kink bands where the fibers were conditioned via the NIJ protocol, referred to as “NIJ/Kink-Bands”; and e) areas with kink bands on fibers that were conditioned via the folding protocol, referred to as “Folding/Kink-Bands”. The results are summarized in Fig. 2 below.

The SEM/EDS results demonstrate a statistically significant (Student’s t-test, $p \leq 0.05$) increase in the oxygen concentrations at the kink band areas of both the NIJ conditioned and folded UHMMPE fibers. This increase can be attributed to the formation of oxidation products, such as esters, ketones, aldehydes, peroxyl radicals, alkoxyl radicals, or an increase of the molecular oxygen concentration produced during the thermo-oxidative degradation of UHMMPE from reactions such as the recombination reaction of peroxyl radicals, as will be discussed later. Also, the relatively high (8.51 ± 0.63 wt. %) initial concentration of molecular oxygen observed on the fibers could be potentially attributed to the manufacturing process of the fibers. More specifically, during the solution spinning step, PE is dissolved in decalin where the solubility of oxygen is relatively high with a value of Henry’s constant (H) equal to 12,700 Pa m^3 mol^{-1} at 20 °C [45]. Another important conclusion from the SEM/EDS results is that areas on the aged fibers without kink bands show similar oxygen concentration to the new, unaged, fibers. These results demonstrate that the oxidation of the UHMMPE fibers mainly occurs in the kink banded areas, which can be explained by considering the potential chemical reactions that can occur in the fiber after the kink band forms. However, since it is very difficult to estimate the number of kink bands across the entire length of a fiber, our EDS results cannot be directly compared with the oxidation index values calculated by the IR analysis of the kink-bands. It is worth mentioning though that the EDS and IR data show similar trends. As previously mentioned, compression forces that produce kink bands when combined with tensile forces generated on the opposite side of the fibers can potentially lead to C-C bond scissions along the backbone of the UHMMPE chains, leading to the formation of the C-centered radicals. These Ccentered free radicals react rapidly with the dissolved molecular oxygen to form corresponding peroxyl radicals, which initiate the first step of the oxidation-degradation processes. The consumption of molecular oxygen in the kink bands would enhance the diffusivity of oxygen to these bands from the surrounding volume. Furthermore, micro voids created by the kink bands could enhance the diffusion and solubility of oxygen into these areas of the fiber; leading to more oxygen available for the C-centered radicals to convert to the peroxyl radicals.

3.3. Oxidation product measurements of the kink-banded regions of UHMMPE fibers

FTIR measurements were performed to quantify the oxidation products in the UHMMPE fibers initiated in the kink band areas. First, the FTIR spectrum of UHMMPE fibers extracted from the center section of the 14th laminate (the middle layer) of a new armor panel was acquired and used as a control in this study (Fig. 3). The characteristic peaks at around 2,916 cm^{-1} and 2,848 cm^{-1} are identified as sp^3 C-H symmetric and asymmetric stretching, at around 1,471 cm^{-1} and 1461 cm^{-1} are assigned to C-H bending, and those at 731 cm^{-1} and 717 cm^{-1} are in-phase and out-of-phase C-H rocking, respectively [46]. When oxidation takes place in UHMMPE, a new peak is formed at around 1,700 cm^{-1}. This peak can be usually resolved into two individual peaks, one with a maximum at approximately 1,735 cm^{-1}, which is assigned to an ester; and another one with a maximum at approximately 1,713 cm^{-1}, which is assigned to a ketone [30].

The units of absorbance are arbitrary. The data are the mean values of 3 different fiber samples, each tested in triplicate. All measurements are of the bulk fiber. In Fig. 4, a representative FTIR spectrum of the oxidation peak at around 1,700 cm^{-1} is shown for UHMMPE fibers extracted from the center part of the 14th laminate of a new body armor (New Fibers), fibers extracted from the edge of the 1st laminate of a NIJ conditioned body armor (NIJ Conditioned Fibers), and fibers from the non-folded area (Normal - Folding) and the folded area (Kink Band - Folding) of laminates conditioned using the folding protocol. For each condition, more than three different fiber samples were tested, and spectra was collected from two different areas of the samples. After the integration of each peak, the oxidation index (OI) was calculated for each condition and presented as mean ± standard error of measurement (S.E.M.). The OI of the UHMMPE fibers was calculated by dividing the peak area at 1,713 cm^{-1} by the reference peak area at 1,472 cm^{-1}, according to equation (1) [16, 17, 47]. The OI values for the fiber samples tested in this study are shown in Table 1.

$$OI = \frac{A_{1713cm^{-1}}}{A_{1472cm^{-1}}} \quad (1)$$

As shown in Fig. 4, the “NIJ Conditioned Fibers” demonstrate the most severe oxidation, since the area under the peak at 1713 cm^{-1} was the largest of the four. There is a statistically significant increase in the oxidation index between fibers extracted from new and NIJ conditioned body armor ($p \leq 0.05$, by Student’s t-test). Furthermore, the area under the peak at 1713 cm^{-1} for the “Normal - Folding” was slightly larger than that of the “New Fibers”. These results are in accordance with the results acquired from the EDS analysis described in the previous section, where the UHMMPE fibers from a non-folded area of the laminates aged with the Folding protocol have not shown a significant increase over the fibers extracted from a new panel. Finally, the area under the oxidation peak of the “Kink Band - Folding” was larger than that of the “New Fibers” and the “Normal - Folding” but lower that the “NIJ Conditioned Fibers”. The calculated OI for these fibers was lower than the “NIJ

Conditioned Fibers," but greater than the other two fiber samples in this set of experiments. These differences are statistically significant as evidenced by $p \leq 0.05$ by a Student's t-test.

C−C ruptures on the backbone of the chain lead directly to degradation and a decrease in the molar mass, as previously described in Section 3.1. However, hydrogen abstraction is another reaction that can also lead to degradation in the presence of oxygen. Although in the absence of oxygen C-centered free radicals undergo crosslinking reactions, in the presence or abundance of oxygen in the kink banded area the reactions of carbon centered radicals with oxygen predominate to produce peroxyl radicals. It is not possible with the available analysis techniques to determine the relative concentrations of free bimolecular oxygen and C-centered radicals specifically in the kink banded regions of the fiber. However, our results indicate that there is an abundance of oxygen in the kink banded regions of the fiber, favoring the oxidation reactions. In addition, the reaction rate constant of alkyl C-centered radicals with oxygen is about 10^9 $mol^{-1}s^{-1}$ [48], which is an order of magnitude greater than the crosslinking reaction rate constant of about 10^8 $mol^{-1}s^{-1}$, further favoring these reactions. The abundance of oxygen in the kink banded areas causes the reactions of carbon centered radicals with oxygen to dominate, producing peroxyl radicals. The peroxyl radicals formed in these reactions are relatively stable in highly oriented UHMMPE, despite the readily available hydrogen atoms in the polymer. This stability is confirmed by studies showing that peroxyl radicals in polyethylene are still present after months at room temperature in the presence of oxygen [35]. The stability of these radicals is further supported by the high activation energy needed for hydrogen abstraction from a nearby UHMMPE molecule by peroxyl radicals, which at room temperature has been reported as high as 108 kJ/mol for another UHMMPE system [35], although lower values have also been reported for lower molar mass polyethylene [49]. However, at elevated temperatures, the rate of the hydrogen abstraction reaction increases significantly (almost doubling with a 10 °C increase in temperature), which has practical implications for the use and ageing of the material. Also, in the kink-banded areas, where polymer chains are not as highly oriented and/or tightly packed as in the rest of the fiber areas, these peroxyl radicals could abstract a hydrogen from an adjacent chain to form hydroperoxides and new alkyl macroradicals, as shown in Fig. 5 [15, 50–52].

The effect of liquid water in the degradation process of UHMMPE fibers is not of major concern in this study, in contrast to previous studies [53], since the laminates in the body armor are protected from water via a sealed external waterproof cover, which is typically used in realworld systems. In addition to that, polyethylene is inherently a very hydrophobic polymer, which is highly resistant to liquid water and humidity. However, upon oxidation of the UHMMPE fibers the material becomes more hydrophilic due to the formation of hydrophilic groups such as ketones, carboxylic acids, alcohols and esters [15, 38, 39]. Hence, trace amounts of water and humidity, as could be introduced to the system during wear as the waterproof cover breaks down, can enhance the oxidation process since increased hydrophilicity will increase the diffusivity of water, especially at the kink banded areas where oxidation is primarily observed. Furthermore, the solubility of oxygen in water is much greater than that in polyethylene. Also, as trace amounts of water diffuse more oxygen into the material along with the water due to the solubility of oxygen in water. Ultimately, the diffusion of trace amounts of water and the presence of higher oxygen

concentration at the kink bands could accelerate the decomposition of hydroperoxides, that form during the oxidation process, as shown by Garton et al. [53].

Fig. 5 shows how the C-centered alkyl radicals in the kink bands react with the molecular oxygen to produce the corresponding peroxyl radicals (reaction 5). This reaction is comparatively faster than the recombination reaction of the alkyl radicals. The most important reaction of peroxyl radicals that propagates the oxidation of the polymer is the abstraction of H atoms from neighboring a chain (reaction 6) producing more C-centered radicals and hydroperoxides (RO_2H). Additionally, peroxyl radicals can decompose, leading to chain scission and the formation of lower molar mass chains, new alkyl radicals, and CO_2 (reaction 7). Hydroperoxides have been shown to be thermally unstable [35], especially at temperatures approaching 70 °C, where the rate of the decomposition reaction begins to obey Arrhenius law [35, 52]. As previously mentioned, UHMMPE fibers used in body armor can be exposed to temperatures of approximately 67 °C or higher, for example, if the armor is left in a closed vehicle on a hot day [30]. This can result in thermal oxidation decomposition reactions that can further induce the degradation of the fibers, since hydroperoxides will decompose (reaction 8) to produce very reactive hydroxyl (•OH) and alkoxyl (RO•) radicals, or ketones (R_2CO) and H_2O molecules [33, 35, 52]. The alkoxyl radical can abstract an H atom to produce alkyl radicals and ROH (reaction 9) and the produced •OH radicals can also abstract H atoms form the polymer backbone to form more alkyl radicals and H_2O (reaction 10). In regions of the fiber where the kink bands are absent (and, therefore, the oxygen concentrations are relatively low) it is expected that alkyl radicals undergo crosslinking and disproportionation reactions (reaction 3 and 4, respectively).

3.4. Bulk crystal morphology of kink-banded UHMMPE fibers

Thermal analysis of UHMMPE fibers was conducted using differential scanning calorimetry (DSC) to evaluate the effects of ageing on the total crystallinity of the material and investigate transitions with the relative amounts of the different crystalline phases. Representative DSC thermograms of UHMMPE fibers extracted from new and NIJ conditioned body armor are presented in Fig. 6. In both cases, the thermograms of UHMMPE fiber samples revealed broad melting peaks with a maximum at ~147 °C. All melting peaks were treated as Gaussian functions and fitted to predefine four different melting peaks. These peaks correspond to various crystal phases including orthorhombic, monoclinic, and hexagonal, as well as a mesophase. However, there is no value reported in the literature for the heat of fusion of a 100% monoclinic or a 100% hexagonal crystalline PE material. Hence, our calculations of the total percent crystallinity of these samples was performed using the ASTM standard value for the theoretical heat of fusion of a 100% orthorhombic crystalline polyethylene (289.3 J/g) [54]. For these UHMMPE fiber samples, the overall percent crystallinity as calculated by this method was nearly unchanged. It is important to note that the fibers do not contain any hexagonal crystals at ambient conditions, as determined by the WAXS analysis. This crystal phase forms in the DSC pan as the fibers are heated under constraint, as previously observed by Wunderlich, et al. [55]. Fibers extracted from a new panel exhibited a total percent crystallinity of 90 % ± 1.0 % (slightly higher than reported by the manufacturer) and those extracted from a NIJ conditioned panel

have a slightly smaller value of 87.8 % ± 1.1 %. These numbers represent mean values with their standard uncertainty calculated by more than 6 thermograms per condition, produced from different fiber samples.

This result could indicate that degradation, and more specifically oxidation, is mainly occurring in the amorphous regions of the fibers and does not significantly affect the crystalline phases of the material. This is also supported by the fact that in highly oriented UHMMPE fibers, oxygen transport takes place almost exclusively through the amorphous regions of the polymer and the crystalline regions provide barriers to impede oxygen flow [37]. The extent of these barriers and their influence on the diffusion of oxygen through the amorphous regions of the polymer depend on the molecular orientation of the polymer chains and their packing density in the highly drawn fibers [37]. As a result, at higher drawing ratios, oxygen permeability and diffusion into the UHMMPE fibers through the sparse amorphous regions is more restricted [56]. More recent results have shown that there is a linear correlation between the solubility of oxygen and the amorphous volume fraction of the polymer, which provides the carrier for the diffusion process, while the permeability and diffusion coefficient demonstrate a more complex behavior which relates to the detailed morphology of the crystalline and amorphous regions, such as their distribution and size [57].

Chain scissions and chemicrystallization effect on UHMMPE fibers

It has been previously reported by Fayolle et al. that in semi-crystalline polymers chain scissions occur mainly in the amorphous areas of the polymer. This will result in the formation of “free” polymer chain-ends, which can integrate into the nearby crystalline phases due to their relatively higher mobility. As a result, the material can undergo a process known as chemicrystallization, previously observed in the thermal oxidation of polyolefins [58–60]. In this study, highly oriented and crystalline UHMMPE fibers contains a significantly smaller fraction of amorphous regions as compared to HDPE or polypropylene. Mechanically and chemically induced chain scissions will decrease the size of the long polymer chains in the material, and in the presence of oxygen will result in products such as aldehydes, ketones, alcohols and esters [15, 38]. These shorter chains are expected to have higher mobility and their hydrophilic chain ends, present mainly in the amorphous areas of the fibers, may integrate into the crystalline phase, as reported by Fayolle et al. [58]. However, our results demonstrate that only approximately 8 % of the fibers is amorphous, which limits the impact of chemicrystallization effect in this system. Also, the significantly higher starting molar mass of the polymer (between 3 and 5 million amu) will further reduce the probability of the formation of small chain segments with sufficient mobility to allow them to diffuse into the crystalline regions of the polymer.

As can be seen from Fig. 6, the endotherms of the UHMMPE fibers used in this study were broad with overlapping regions between 136 °C and 162 °C. After the deconvolution of the endotherms into four peaks, these peaks were integrated to give four different areas, and the percentage of the area of the total melting endotherm was attributed to the area of each individual peak. Each one of the deconvolved peaks corresponds to four different melting points, the results of which are summarized in Table 1. The lowest melting peak in the

region of 136 °C is assigned as T_{m1} and is relatively broad. This peak did not change significantly between the new and conditioned vest fibers and is attributed to the melting of the monoclinic phase [12, 61–63]. The second melting peak T_{m2}, around the region of 147 °C is the strongest signal and is attributed to melting of the extended orthorhombic crystals to form pseudo-hexagonal crystals [2, 12, 61, 62, 64, 65]. This peak did not shift between fibers extracted from new and NIJ conditioned body armor. However, the percentage of peak area for the heat of melting decreased from 76.7 % to 70.4 % with ageing. The third melting peak, T_{m3}, is located at around 154 °C and is hypothesized to be the melting of a pseudo-hexagonal mesophase [2, 12, 61, 62, 64, 65]. Finally, a fourth melting peak, T_{m4}, was observed at around 160 °C, which is identified to be the melting of the hexagonal crystal phase [12, 61–64].

These results indicate that the percentages of the monoclinic and the hexagonal crystal phases do not change upon ageing. Prior work has shown that monoclinic crystals can form only at high drawing ratios, whereas hexagonal crystals will only form when polymer chains in UHMMPE fibers are constrained when heated at elevated temperatures, such as in the case of fiber drawing at high temperatures [66, 67]. Therefore, the presence of these two crystal phases in these fibers further validates that the fibers used in this body armor are highly drawn fibers with very highly oriented polymer chains, as expected. Also, ageing of the body armor at 65 °C is not a high enough temperature to melt the monoclinic crystal phase, as shown by these DSC results. Thus, the percentage of this phase did not change upon ageing, as expected.

The most significant change observed from the thermal analysis of these samples is the decrease of the orthorhombic crystal phase after ageing, as shown in Table 3. Changes in the orthorhombic crystal phase are most evident because of its relative abundance (almost 80 % of the polymer chains form orthorhombic crystals) in the material. Without any significant changes to the other two crystal phases identified (monoclinic and hexagonal), these results may suggest that during ageing, some polymer chains originally in the orthorhombic crystal phase are losing their initial conformation. This allows these polymer chains to re-orient and convert more easily into crystalline intermediate phase (mesophase) between the transitions of the polymer chains from the orthorhombic to the hexagonal crystals. This hypothesis could be explained if one considers the parameters of the formation of the hexagonal phase. The hexagonal crystal phase will form upon heating the polymer chains at high temperatures (150 °C, or higher) while constraining them at the same time [66]. The drawing process used to make the fibers examined in this study results in very low free volume between the polymer chains in the extended orthorhombic phase [68, 69]. Therefore, upon heating during the DSC analysis, the chains in the orthorhombic phase might not be able to fold back on each other, since they are constrained by the adjacent chains, and may form pseudo-hexagonal and hexagonal crystals, as shown by the DSC endotherms [63]. However, as temperature increases in the DSC pan, the freedom of motion and free volume of the self-constrained polymer chains will increase. Therefore, the conditions are not optimum for the complete transformation of the orthorhombic to a hexagonal phase, and a new mesophase, which could have some orthorhombic and some hexagonal phase properties, can potentially form.

The UHMMPE fibers used in this study were shown to be very highly crystalline with about 90% total crystallinity. This results in very tightly packed and highly oriented crystallites within the fibers. To better understand the morphological changes that the crystals undergo in the material we need to fully characterize the crystal morphology of these fibers. In this set of experiments, WAXS analysis was performed on UHMMPE fibers extracted from new body armor panels to assess the different type of crystals initially present in these fibers, and complement the data obtained from the DSC analysis. WAXS data of the new fibers were collected at 25 °C and 140 °C to further our understanding of the DSC results. The diffraction patterns are shown in Fig. 7, and the diffractograms of intensity vs. 2θ° are shown in Fig. 8 and Fig. 9.

As can be seen from the figures above, two monoclinic peaks and two orthorhombic peaks are identified for the fibers extracted from new vests at 25 °C [14, 63, 67, 70]. As the temperature increases to 140 °C, the monoclinic (001) diffraction peak can be barely detected, while the area under the (20–1) monoclinic peak decreases from 1.79 %, in the 25 °C diffractogram, to 1.44 %. Overall, the percentage of the monoclinic phase decreases from 2.22 % to 1.44 % as temperature increases from 25 °C to 140 °C. This result indicates that some phenomenon is occurring at a temperature between this range to cause the monoclinic phase to decrease, supporting the interpretation of the DSC results where the melting peak at 136 °C was assigned to the monoclinic phase. Also, at room temperature the amount of the monoclinic phase calculated by the deconvolution of the DSC endotherm was found to be ~ 2 %, which is in agreement with the value of 2.22 % calculated by the integration of the WAXS diffraction patterns of $(001)_m$ and $(20–1)_m$ at 25 °C. Finally, no hexagonal phase was observed in the WAXS diffractograms of the fibers, since the appearance of the WAXS diffraction peak of the hexagonal phase has been shown to occur at temperatures above 150 °C under constraint [62]. The equatorial diffraction peak of the hexagonal phase is expected at $2_\theta = 20.5°$ [63]. Since the diffraction peak of the (110) lattice plane of the orthorhombic crystals is at $2\theta = 21.5°$, observing the diffraction peak of such a small percentage (only ~1 %) of hexagonal phase due to overlapping of the two peaks is challenging. However, if WAXS analysis is conducted on constrained fibers at very high temperatures (above 150 °C), the intensity of the diffraction peak of the hexagonal phase at $2\theta = 20.5°$ will be strong and easily identified [62]. Additionally, the meridional diffraction pattern of the crystals when fibers are placed perpendicular to the X-ray beam, which could potentially reveal the existence of the pseudo-hexagonal phase, was not collected in this study due to lack of an appropriate mounting stage but will be considered for future work.

3.5. Free radical identification

EPR spectroscopy has been used to identify the structures of the polyethylene alkyl, allyl, polyenyl, peroxyl, and alkoxyl radicals [71–75]. Fig. 10 shows the EPR spectrum of the free radicals in the kink-banded areas of an aged sample approximately one year after ageing was discontinued. Under our experiment ageing conditions, the thermo-mechanically-produced reducing-alkyl C-centered radicals react rapidly with molecular oxygen to produce their corresponding peroxyl radicals. The reaction rate constant for this reaction is approximately 2.9×10^9 L mol^{-1} s^{-1} to 4.7×10^9 L mol^{-1} s^{-1} [76]. Therefore, it is difficult to detect their sextet signal in the aged UHMMPE samples [77, 78] using our experimental arrangement.

However, the peroxyl and alkoxyl radicals undergo various reactions leading to the formation of organic peroxides and scissions of the backbone of the UHMMPE chains as shown in Fig. 5. Hence, it is not surprising to observe a relatively small concentration of long-lived alkoxyl and peroxyl radicals in the kink-banded areas of the fibers.

The EPR spectrum in Fig. 10 displays signals suggesting the presence of the unpaired electron on the oxygen atoms of the molecules [79]. The hyperfine splitting pattern of the EPR spectrum can be calculated by the following general formula: $(2M_1I_1+1)$ = number of the hyperfine lines, where M is the number of the adjacent H atoms, and I is spin 1= ½ [79]. Since the nearest number of adjacent H atoms in the peroxyl and alkoxyl radicals is one, it is expected that the number of the hyperfine lines is 2. The spectrum in Fig. 10 shows a signal with a pattern of 2 EPR hyperfine lines, in addition to other very small-amplitude lines. Based on frequency of 9.434849GHz, and B values of 3315.9 G, 3361.3G, and 3367.2G, the g-factors were found to be 2.032, 2.005, and 2.002 respectively. These values agree fairly well with the published values of peroxyl radicals reported by Fel et al. as well and Jahan [71, 74]. It should also be mentioned that the EPR signal may include a small contribution from the fast reacting alkoxyl and long-lived polyenyl radicals. The presence of the EPR signal in the kink-banded regions, even after one year of discontinuing aging, is worthy of attention. This suggests that the oxidation reactions shown in Fig. 5 are still taking place. As expected, prior work has shown that unaged UHMMPE fibers of the same type do not exhibit any EPR signal prior to ageing [80].

4. Summary

The results of this study have demonstrated the enhancement of the oxidation reactions in the kink-banded areas of the UHMMPE fibers. Under aerobic conditions, the combination of the thermo-mechanical stress and the presence of water (80 % RH) enhance degradation through the oxidation reactions in the kink-banded areas. As a result, the FTIR and EDS show that the concentrations of oxygen-containing compounds are more pronounced in the kink band region than in the unkinked regions of the fiber. Oxidation is enhanced in the kink-band regions because of the a) higher O_2 concentrations caused by the void formation within those regions and b) the decrease in the orthorhombic crystal structure from 77 % to 70 %, which results in an increase of the O_2 diffusion rate of from the surrounding environment into the kink band area.

Our results also show that no significant changes were observed to the other two crystalline phases identified (monoclinic and hexagonal) during ageing. These results may suggest that during ageing, some polymer chains originally in the orthorhombic crystal phase are losing their initial conformation. This allows these polymer chains to re-orient and convert more easily into a pseudo-hexagonal crystal phase, which is a mesophase between the transitions of the polymer chains from the orthorhombic to the hexagonal crystals.

Finally, the EPR results have revealed that even after one year of removing the vests from the ageing chamber and extracting the UHMMPE fibers, alkoxyl and peroxyl radicals persist in the kink band region. This indicates that the oxidation and the degradation reactions take place even after discontinuing the exposure of these fibers to the thermo-mechanical stress.

Therefore, it is critical to protect armor containing UHMMPE fibers from heat and bending damage, and humidity exposure to the extent possible, as these conditions may reduce its strength and effectiveness.

References

[1]. Mann G, Encyclopedia of polymer science and engineering, Acta Polymerica 40(2) (1989) 137–138.

[2]. Li C-S, Zhan M-S, Huang X-C, Zhou H, Degradation behavior of ultra-high molecular weight polyethylene fibers under artificial accelerated weathering, Polymer Testing 31(7) (2012) 938–943.

[3]. Chin J, Petit S, Forster A, Riley M, Rice K, Effect of artificial perspiration and cleaning chemicals on the mechanical and chemical properties of ballistic materials, Journal of Applied Polymer Science 113(1) (2009) 567–584.

[4]. Fisch AG, da Silveira N, Cardozo NSM, Secchi AR, dos Santos JHZ, Soares JBP, Direct production of ultra-high molecular weight polyethylene with oriented crystalline microstructures, Journal of Molecular Catalysis A: Chemical 366 (2013) 74–83.

[5]. Tompkins D, Body Armor Safety Initiative: To Protect and Serve... Better, NIJ Journal 254 (2006).

[6]. Kurtz SM, Muratoglu OK, Evans M, Edidin AA, Advances in the processing, sterilization, and crosslinking of ultra-high molecular weight polyethylene for total joint arthroplasty, Biomaterials 20(18) (1999) 1659–1688. [PubMed: 10503968]

[7]. Kurtz SM, UHMWPE biomaterials handbook: ultra high molecular weight polyethylene in total joint replacement and medical devices, Academic Press2009.

[8]. Kurtz SM, The UHMWPE handbook: ultra-high molecular weight polyethylene in total joint replacement, Academic press2004.

[9]. Smook J, Pennings AJ, Preparation of ultra-high strength polyethylene fibres by gel-spinning/hotdrawing at high spinning rates, Polymer Bulletin 9(1–3) (1983).

[10]. Kanamoto T, Tsuruta A, Tanaka K, Takeda M, Porter RS, Super-drawing of ultrahigh molecular weight polyethylene. 1. Effect of techniques on drawing of single crystal mats, Macromolecules 21(2) (1988) 470–477.

[11]. Ottani S, Ferracini E, Ferrero A, Malta V, Porter RS, SAXS investigations on uniaxially drawn fibers obtained from polyethylene reactor powder, Macromolecules 29(9) (1996) 3292–3299.

[12]. Ratner S, Weinberg A, Wachtel E, Moret P, Marom G, Phase transitions in UHMWPE fiber compacts studied by in situ synchrotron microbeam WAXS, Macromolecular rapid communications 25(12) (2004) 1150–1154.

[13]. Fu Y, Chen W, Pyda M, Londono D, Annis B, Boller A, Habenschuss A, Cheng J, Wunderlich B, Structure-property analysis for gel-spun, ultrahigh molecular mass polyethylene fibers, Journal of Macromolecular Science, Part B 35(1) (1996) 37–87.

[14]. Litvinov VM, Xu J, Melian C, Demco DE, Möller M, Simmelink J, Morphology, Chain Dynamics, and Domain Sizes in Highly Drawn Gel-Spun Ultrahigh Molecular Weight Polyethylene Fibers at the Final Stages of Drawing by SAXS, WAXS, and1H Solid-State NMR, Macromolecules 44(23) (2011) 9254–9266.

[15]. Schnabel W, Polymer degradation : principles and practical applications, Hanser International, New York, 1981.

[16]. Forster AL, Forster AM, Chin JW, Peng J-S, Lin C-C, Petit S, Kang K-L, Paulter N, Riley MA, Rice KD, Al-Sheikhly M, Long-term stability of UHMWPE fibers, Polymer Degradation and Stability 114 (2015) 45–51.

[17]. Costa L, Luda M, Trossarelli L, Ultra-high molecular weight polyethylene: I. Mechano-oxidative degradation, Polymer degradation and stability 55(3) (1997) 329–338.

[18]. Takahashi T, Miura M, Sakurai K, Deformation band studies of axially compressed poly (p-phenylene terephthalamide) fiber, Journal of Applied Polymer Science 28(2) (1983) 579–586.

[19]. Edmunds R, Wadee MA, On kink banding in individual PPTA fibres, Composites Science and Technology 65(7) (2005) 1284–1298.

[20]. Hunt GW, Peletier MA, Wadee MA, The Maxwell stability criterion in pseudo-energy models of kink banding, Journal of Structural Geology 22(5) (2000) 669–681.

[21]. Silverstein M, Breuer O, Dodiuk H, Surface modification of UHMWPE fibers, Journal of Applied Polymer Science 52(12) (1994) 1785–1795.

[22]. Dobb M, Johnson D, Saville B, Compressional behaviour of Kevlar fibres, Polymer 22(7) (1981) 960–965.

[23]. Leal AA, Deitzel JM, Gillespie JW, Compressive strength analysis for high performance fibers with different modulus in tension and compression, Journal of composite materials 43(6) (2009) 661674.

[24]. Lorenzo-Villafranca E, Tamargo-Martínez K, Molina-Aldareguia JM, González C, MartínezAlonso A, Tascón JMD, Gracia M, Llorca J, Influence of plasma surface treatments on kink band formation in PBO fibers during compression, Journal of Applied Polymer Science 123(4) (2012) 20522063.

[25]. Attwood J, Fleck N, Wadley H, Deshpande V, The compressive response of ultra-high molecular weight polyethylene fibres and composites, International Journal of Solids and Structures 71 (2015) 141155.

[26]. Attwood J, Khaderi S, Karthikeyan K, Fleck N, Wadley H, Deshpande V, The out-of-plane compressive response of Dyneema® composites, Journal of the Mechanics and Physics of Solids 70 (2014) 200–226.

[27]. Liu G, Thouless M, Deshpande V, Fleck N, Collapse of a composite beam made from ultra high molecular-weight polyethylene fibres, Journal of the Mechanics and Physics of Solids 63 (2014) 320–335.

[28]. Hazzard MK, Hallett S, Curtis PT, Iannucci L, Trask RS, Effect of fibre orientation on the low velocity impact response of thin Dyneema® composite laminates, International Journal of Impact Engineering 100 (2017) 35–45.

[29]. Fleck N, Compresssive failure of fiber composites, Advances in applied mechanics 33(43) (1997) 117.

[30]. Forster AL, Rice KD, Riley MA, Messin G, Petit S, Clerici C, Vigoroux M, Pintus P, Holmes G, Chin J, Development of soft armor conditioning protocols for NIJ standard-0101.06: Analytical results, National Institute of Standards and Technology (2009).

[31]. Stadler FJ, Kaschta J, Münstedt H, Dynamic-mechanical behavior of polyethylenes and ethene-/αolefin-copolymers. Part I. α′-Relaxation, Polymer 46(23) (2005) 10311–10320.

[32]. Gedde U, Polymer physics, Springer Science & Business Media 2013.

[33]. Coote CF, Hamilton JV, McGimpsey WG, Thompson RW, Oxidation of gamma-irradiated ultrahigh molecular weight polyethylene, Journal of applied polymer science 77(11) (2000) 2525–2542.

[34]. Gates BC, Katzer JR, Schuit GC, Chemistry of catalytic processes, McGraw-Hill New York 1979.

[35]. Costa L, Bracco P, Mechanisms of crosslinking, oxidative degradation and stabilization of UHMWPE, UHMWPE Biomaterials Handbook (2009) 309.

[36]. Pauly S, Permeability and Diffusion Data in Polymer Handbook, edited by Brandrup J, Immergut EH, Wiley Interscience, New York, 1989.

[37]. Michaels AS, Bixler HJ, Solubility of gases in polyethylene, Journal of Polymer Science 50(154) (1961) 393–412.

[38]. Collier JP, Sperling DK, Currier JH, Sutula LC, Saum KA, Mayor MB, Impact of gamma sterilization on clinical performance of polyethylene in the knee, The Journal of arthroplasty 11(4) (1996) 377–389. [PubMed: 8792243]

[39]. Lazár M, Free radicals in chemistry and biology, CRC press 1989.

[40]. Grujicic M, Arakere G, He T, Bell WC, Cheeseman BA, Yen CF, Scott B, A ballistic material model for cross-plied unidirectional ultra-high molecular-weight polyethylene fiber-reinforced armorgrade composites, Materials Science and Engineering: A 498(1–2) (2008) 231–241.

[41]. Park AD, Park D, Park AJ, Ballistic laminate structure in sheet form, Google Patents, 2006.

[42]. Park AD, Ballistic panel, Google Patents, 1995.

[43]. Gulmine J, Janissek P, Heise H, Akcelrud L, Polyethylene characterization by FTIR, Polymer Testing 21(5) (2002) 557–563.

[44]. Snavely D, Dubsky J, Near-IR spectra of polyethylene, polyethylene glycol, and polyvinylethyl ether, Journal of polymer science part A: polymer chemistry 34(13) (1996) 2575–2579.

[45]. Luehring P, Schumpe A, Gas solubilities (hydrogen, helium, nitrogen, carbon monoxide, oxygen, argon, carbon dioxide) in organic liquids at 293.2 K, Journal of Chemical and Engineering Data 34(2) (1989) 250–252.

[46]. Teodoru S, Kusano Y, Rozlosnik N, Michelsen PK, Continuous Plasma Treatment of Ultra-High-Molecular-Weight Polyethylene (UHMWPE) Fibres for Adhesion Improvement, Plasma Processes and Polymers 6(S1) (2009) S375–S381.

[47]. Tashiro K, Sasaki S, Kobayashi M, Structural investigation of orthorhombic-to-hexagonal phase transition in polyethylene crystal: the experimental confirmation of the conformationally disordered structure by X-ray diffraction and infrared/Raman spectroscopic measurements, Macromolecules 29(23) (1996) 7460–7469.

[48]. Marchaj A, Kelley DG, Bakac A, Espenson JH, Kinetics of the reactions between alkyl radicals and molecular oxygen in aqueous solution, The Journal of Physical Chemistry 95(11) (1991) 4440–4441.

[49]. Denisov ET, Afanas' ev IB, Oxidation and antioxidants in organic chemistry and biology, CRC press 2005.

[50]. Lacoste J, Carlsson D, Gamma-, photo-, and thermally-initiated oxidation of linear low density polyethylene: A quantitative comparison of oxidation products, Journal of Polymer Science Part A: Polymer Chemistry 30(3) (1992) 493–500.

[51]. Lacoste J, Carlsson D, Falicki S, Wiles D, Polyethylene hydroperoxide decomposition products, Polymer degradation and stability 34(1–3) (1991) 309–323.

[52]. Woods RJ, Pikaev AK, Applied radiation chemistry: radiation processing, John Wiley & Sons 1994.

[53]. Henry JL, Ruaya AL, Garton A, The kinetics of polyolefin oxidation in aqueous media, Journal of Polymer Science Part A: Polymer Chemistry 30(8) (1992) 1693–1703.

[54]. ASTMF2625, Standard Test Method for Measurement ofEnthalpy of Fusion, Percent Crystallinity, and Melting Pointof Ultra-High-Molecular Weight Polyethylene by Means ofDifferential Scanning Calorimetry, 2010.

[55]. Gaur U, Wunderlich B, Heat capacity and other thermodynamic properties of linear macromolecules. II. Polyethylene, Journal of Physical and Chemical Reference Data 10(1) (1981) 119152.

[56]. Capaccio G, Ward I, Structural studies of ultrahigh-modulus linear polyethylene using nitric acid etching and gel permeation chromatography. I. Determination of the crystal size distribution, Journal of Polymer Science: Polymer Physics Edition 19(4) (1981) 667–675.

[57]. Holden P, Orchard G, Ward I, A study of the gas barrier properties of highly oriented polyethylene, Journal of Polymer Science: Polymer Physics Edition 23(4) (1985) 709–731.

[58]. Fayolle B, Richaud E, Colin X, Verdu J, degradation-induced embrittlement in semi-crystalline polymers having their amorphous phase in rubbery state, Journal of materials science 43(22) (2008) 6999–7012.

[59]. Fayolle B, Richaud E, Verdu J, Farcas F, Embrittlement of polypropylene fibre during thermal oxidation, Journal of materials science 43(3) (2008) 1026–1032.

[60]. Winslow F, Aloisio C, Hawkins W, Matreyek W, Matsuoka S, DEPENDENCE OF POLYOLEFIN OXIDATION ON MORPHOLOGY, CHEMISTRY & INDUSTRY (13) (1963) 533–534.

[61]. Hu X-D, Jenkins SE, Min BG, Polk MB, Kumar S, Rigid-Rod Polymers: Synthesis, Processing, Simulation, Structure, and Properties, Macromolecular Materials and Engineering 288(11) (2003) 823843.

[62]. Rein DM, Shavit L, Khalfin RL, Cohen Y, Terry A, Rastogi S, Phase transitions in ultraoriented polyethylene fibers under moderate pressures: A synchrotron X-ray study, Journal of Polymer Science Part B: Polymer Physics 42(1) (2004) 53–59.

[63]. Kwon Y, Boller A, Pyda M, Wunderlich B, Melting and heat capacity of gel-spun, ultra-high molar mass polyethylene fibers, Polymer 41(16) (2000) 6237–6249.

[64]. Devaux E, Cazé C, Composites of UHMW polyethylene fibres in a LD polyethylene matrix. I. Processing conditions, Composites science and technology 59(3) (1999) 459–466.

[65]. Smith P, Lemstra PJ, Kalb B, Pennings AJ, Ultrahigh-strength polyethylene filaments by solution spinning and hot drawing, Polymer Bulletin 1(11) (1979) 733–736.

[66]. Garcia-Leiner M, Song J, Lesser AJ, Drawing of ultrahigh molecular weight polyethylene fibers in the presence of supercritical carbon dioxide, Journal of Polymer Science Part B: Polymer Physics 41(12) (2003) 1375–1383.

[67]. Yeh J-T, Lin S-C, Tu C-W, Hsie K-H, Chang F-C, Investigation of the drawing mechanism of UHMWPE fibers, Journal of Materials Science 43(14) (2008) 4892–4900.

[68]. Smook J, Pennings J, Influence of draw ratio on morphological and structural changes in hotdrawing of UHMW polyethylene fibres as revealed by DSC, Colloid and Polymer Science 262(9) (1984) 712–722.

[69]. Peterlin A, Drawing and extrusion of semi-crystalline polymers, Colloid and polymer science 265(5) (1987) 357–382.

[70]. Ratner S, Weinberg A, Wachtel E, Moret PM, Marom G, Phase Transitions in UHMWPE Fiber Compacts Studied by in situ Synchrotron Microbeam WAXS, Macromolecular Rapid Communications 25(12) (2004) 1150–1154.

[71]. Fel E, Khrouz L, Massardier V, Bonneviot L, Comparative study of gamma-irradiated PP and PE polyolefins part 1: Identification and quantification of radicals using electron paramagnetic resonance, Polymer 77 (2015) 278–288.

[72]. Buttafava A, Tavares A, Arimondi M, Zaopo A, Nesti S, Dondi D, Mariani M, Faucitano A, Dose rate effects on the radiation induced oxidation of polyethylene, Nuclear Instruments and Methods in Physics Research Section B: Beam Interactions with Materials and Atoms 265(1) (2007) 221–226.

[73]. Svistunenko DA, An EPR study of the peroxyl radicals induced by hydrogen peroxide in the haem proteins, Biochimica et Biophysica Acta (BBA)-Protein Structure and Molecular Enzymology 1546(2) (2001) 365–378. [PubMed: 11295442]

[74]. Jahan MS, ESR insights into macroradicals in UHMWPE, UHMWPE Biomaterials Handbook (Third Edition), Elsevier 2015, pp. 668–692.

[75]. Jahan MS, Durant J, Investigation of the oxygen-induced radicals in ultra-high molecular weight polyethylene, Nuclear Instruments and Methods in Physics Research Section B: Beam Interactions with Materials and Atoms 236(1–4) (2005) 166–171.

[76]. Ross AB, Neta P, Rate constants for reactions of aliphatic carbon-centered radicals in aqueous solution, NATIONAL STANDARD REFERENCE DATA SYSTEM, 1982.

[77]. Kasser MJ, Silverman J, Al-Sheikhly M, EPR simulation of polyenyl radicals in ultrahigh molecular weight polyethylene, Macromolecules 43(21) (2010) 8862–8867.

[78]. Kasser MJ, Silverman J, Al-Sheikhly M, On the mechanism of polyenyl photoconversion in irradiated ultrahigh molecular weight polyethylene, Macromolecules 43(21) (2010) 8868–8873.

[79]. Rieger P, Electron spin resonance: analysis and interpretation, Royal Society of Chemistry 2007.

[80]. Forster AL, Long term stability and implications for performance of high strength fibers used in body armor, University of Maryland, College Park 2012.

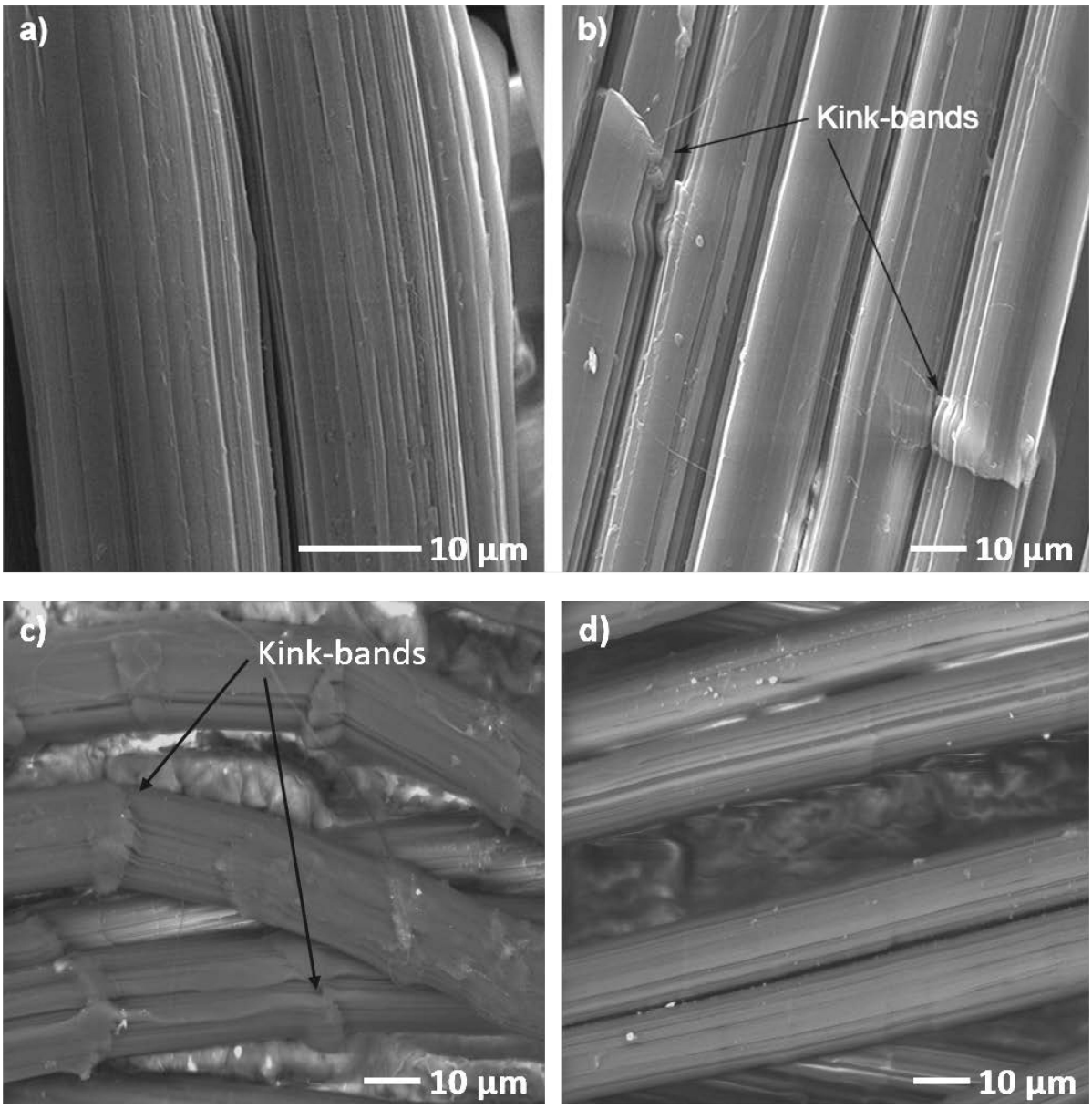

Fig. 1.

Scanning electron microscopy (SEM) images of UHMMPE fibers extracted from new (a), NIJ-ageing protocol (b), and armor panels aged via the folding protocol, 180° bending point (c) and non-bended areas (d) respectively.

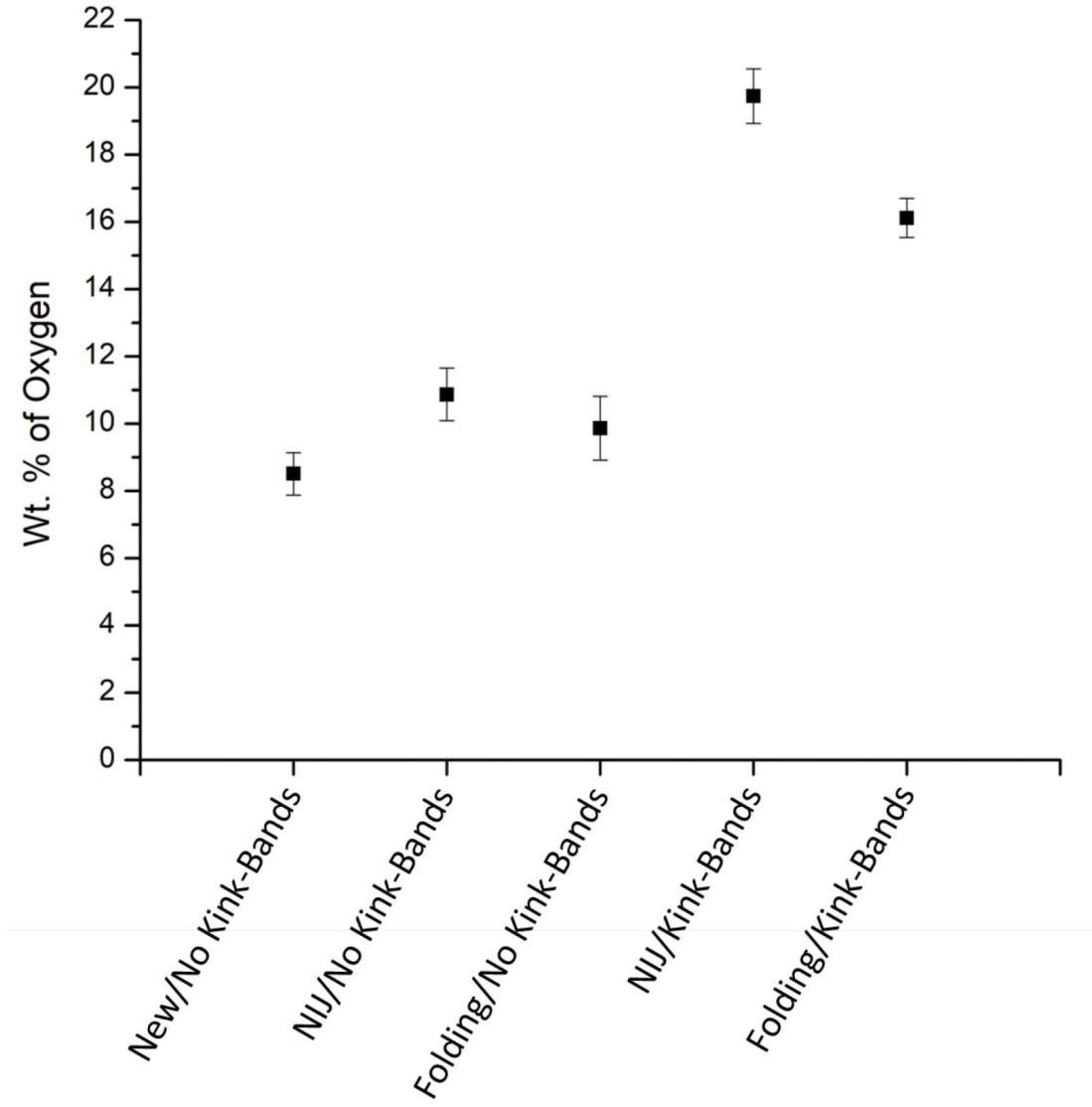

Fig. 2.

EDS analysis on UHMMPE fibers extracted from new and aged body armor through the NIJ and Folding protocols. For each fiber sample, the normalized wt.% of oxygen is reported. Data are mean ± Standard Error of Measurement (S.E.M.) (n≥50).

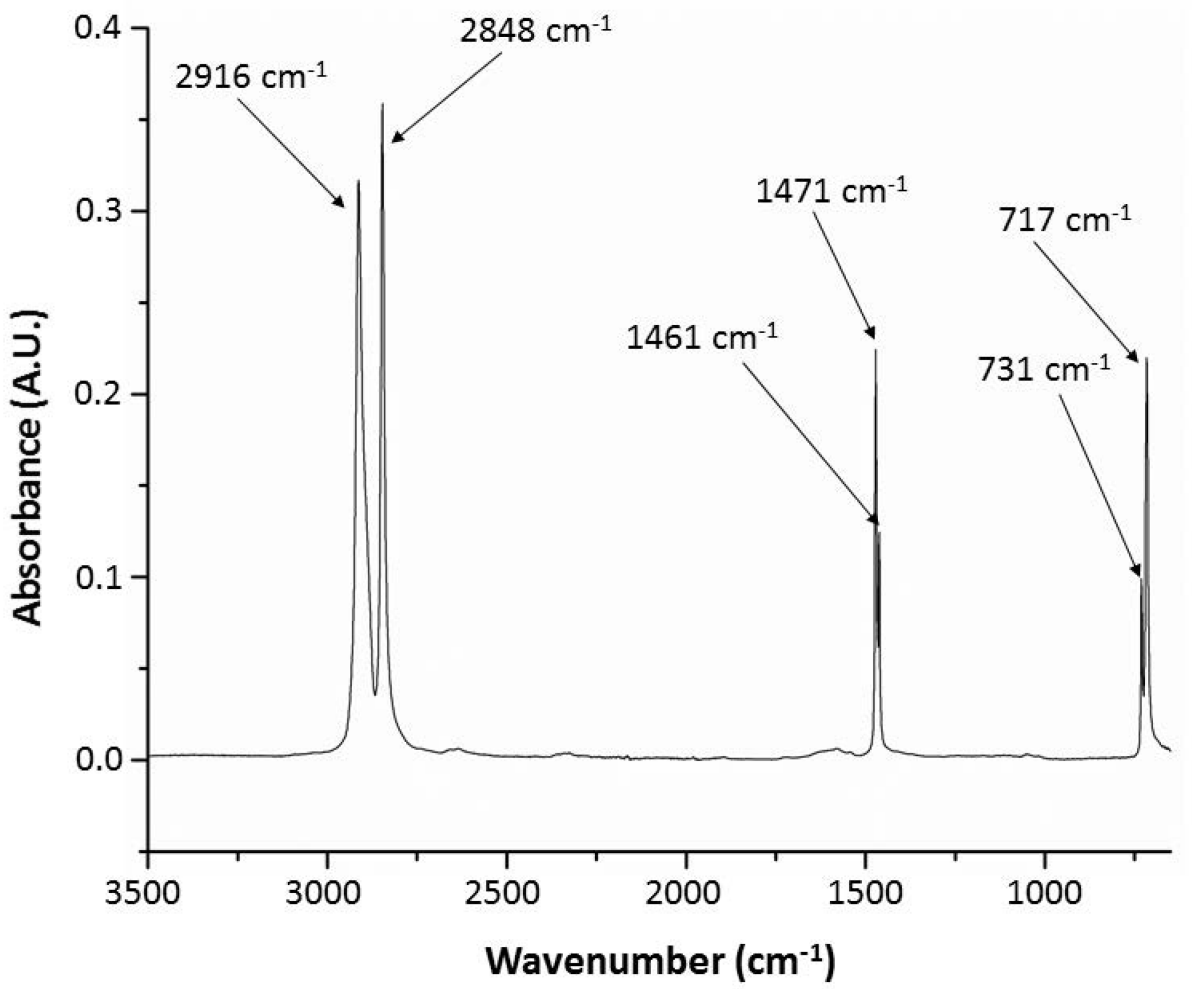

Fig. 3.

FTIR spectrum of control UHMMPE fibers, extracted from the center panel of an unaged armor

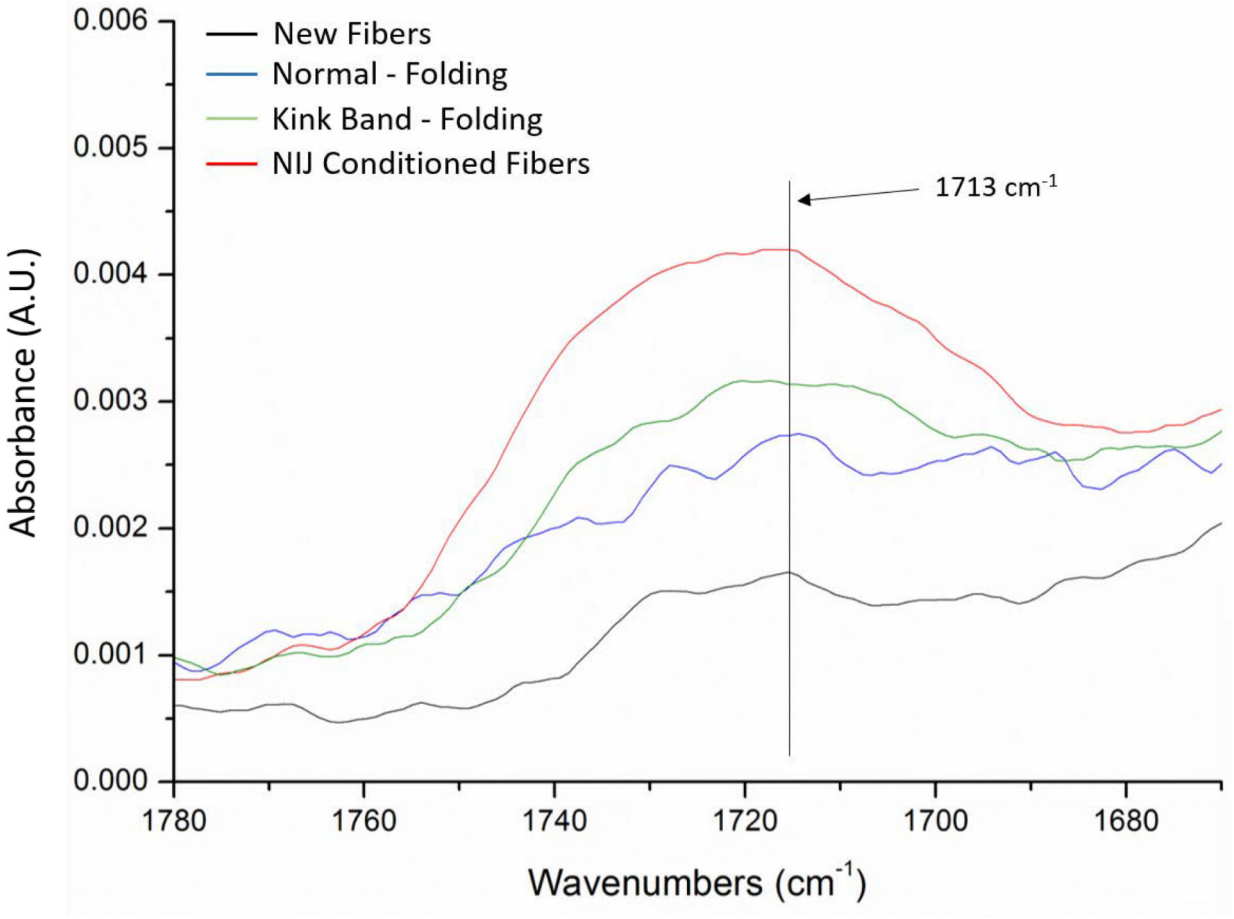

Fig. 4.

FTIR spectra of the oxidation peak at 1,713 cm^{-1} wavenumbers for different UHMMPE fiber samples. These peaks were integrated between 1,690 cm^{-1} and 1,755 cm^{-1} and the areas calculated were used to calculate the OI of the samples.

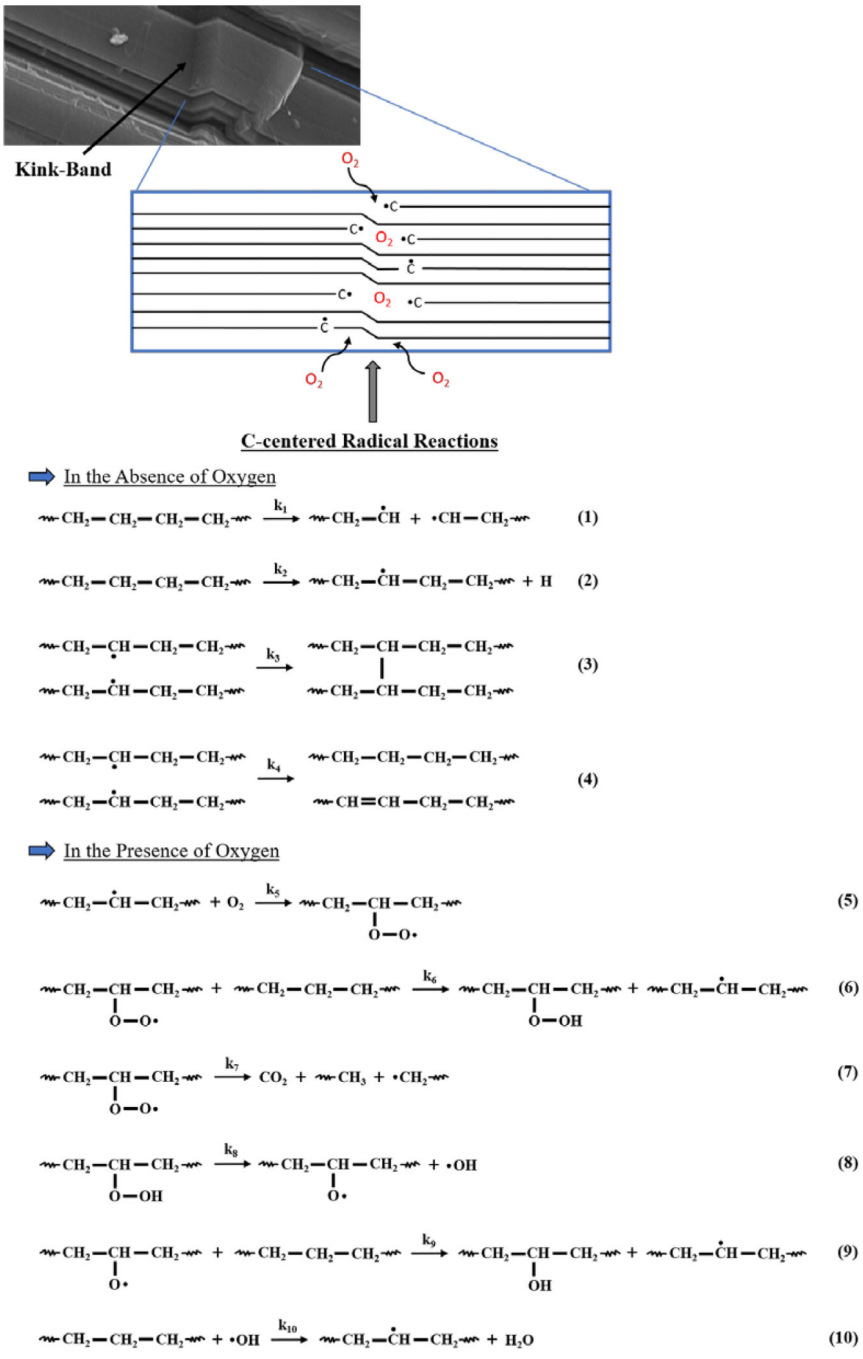

Fig. 5.

The most probable reactions of C-centered radicals in the presence and absence of oxygen in the kink bands.

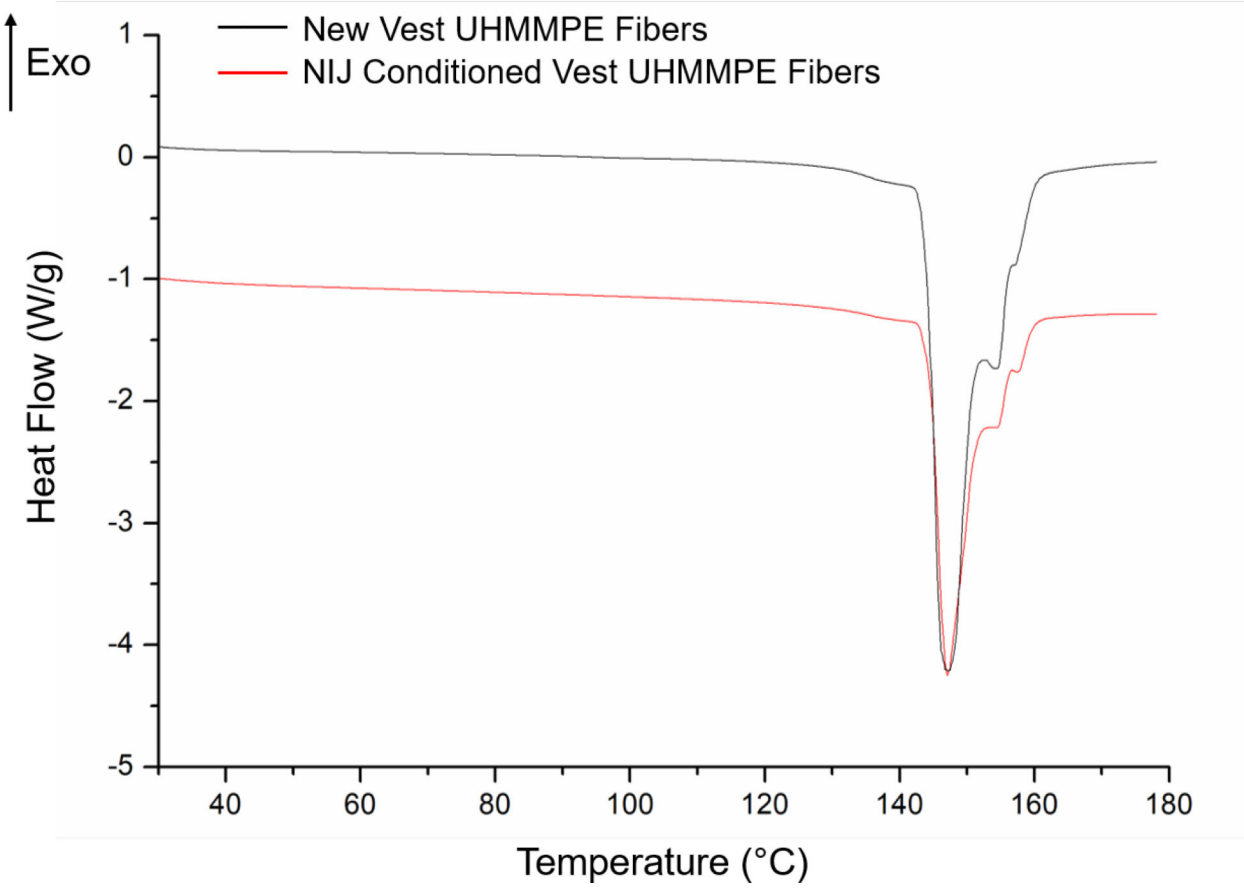

Fig. 6.

DSC thermograms of UHMMPE fibers extracted from a new armor panel (red) and one conditioned with the NIJ protocol (black). Note the broad melting curve, which can be resolved into four individual peaks with different maximum temperatures and different intensities. Standard uncertainties associated with the use of DSC in the measurement of these thermal properties are approximately 5 %.

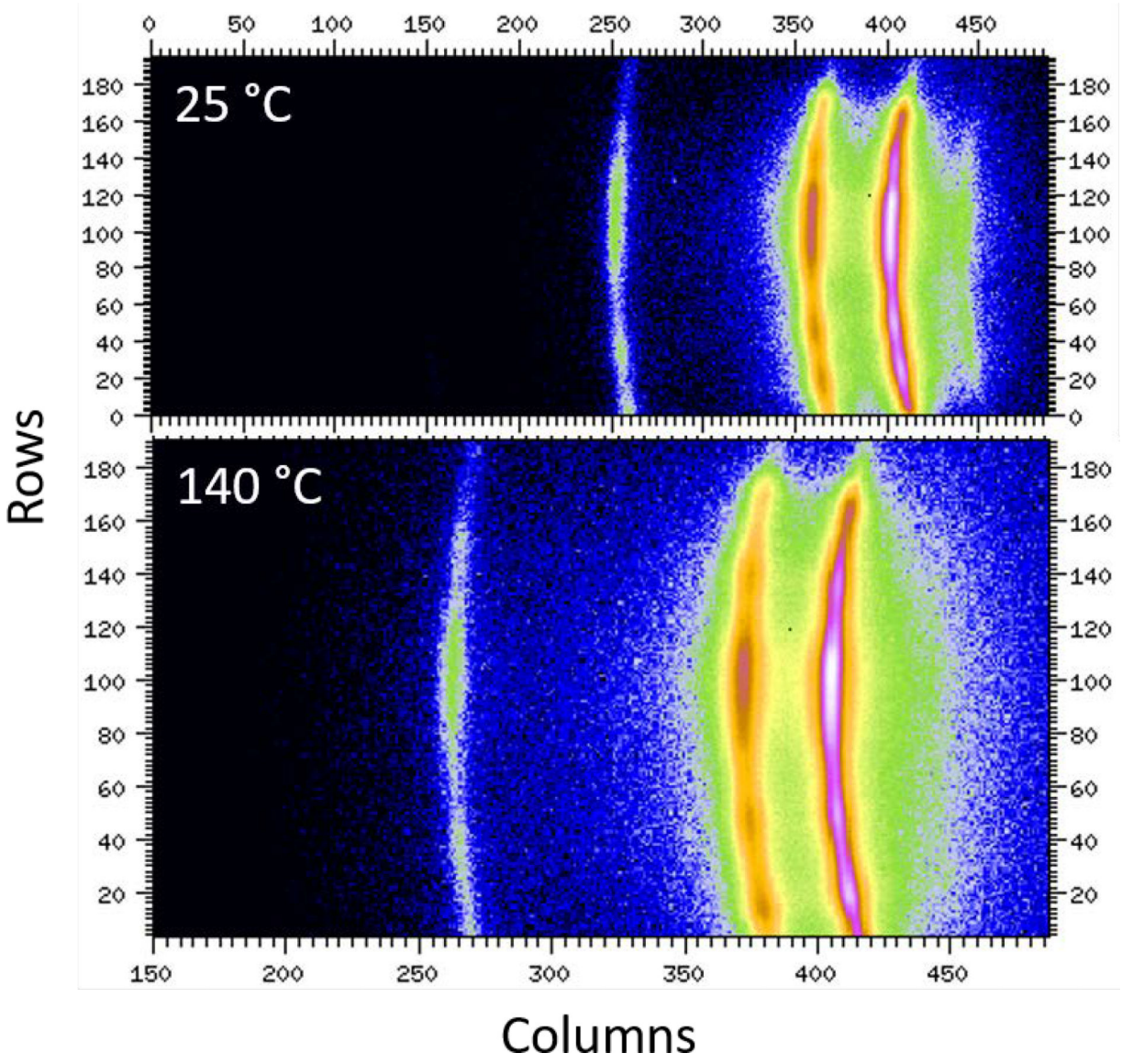

Fig. 7.

2D WAXS patterns for UHMMPE fibers extracted from new vests at about 25 °C and 140 °C. The scattering patterns were measured on a bundle of fibers placed horizontally, with their axis perpendicularly to the X-ray beam. Each condition was measured twice using different samples on different days.

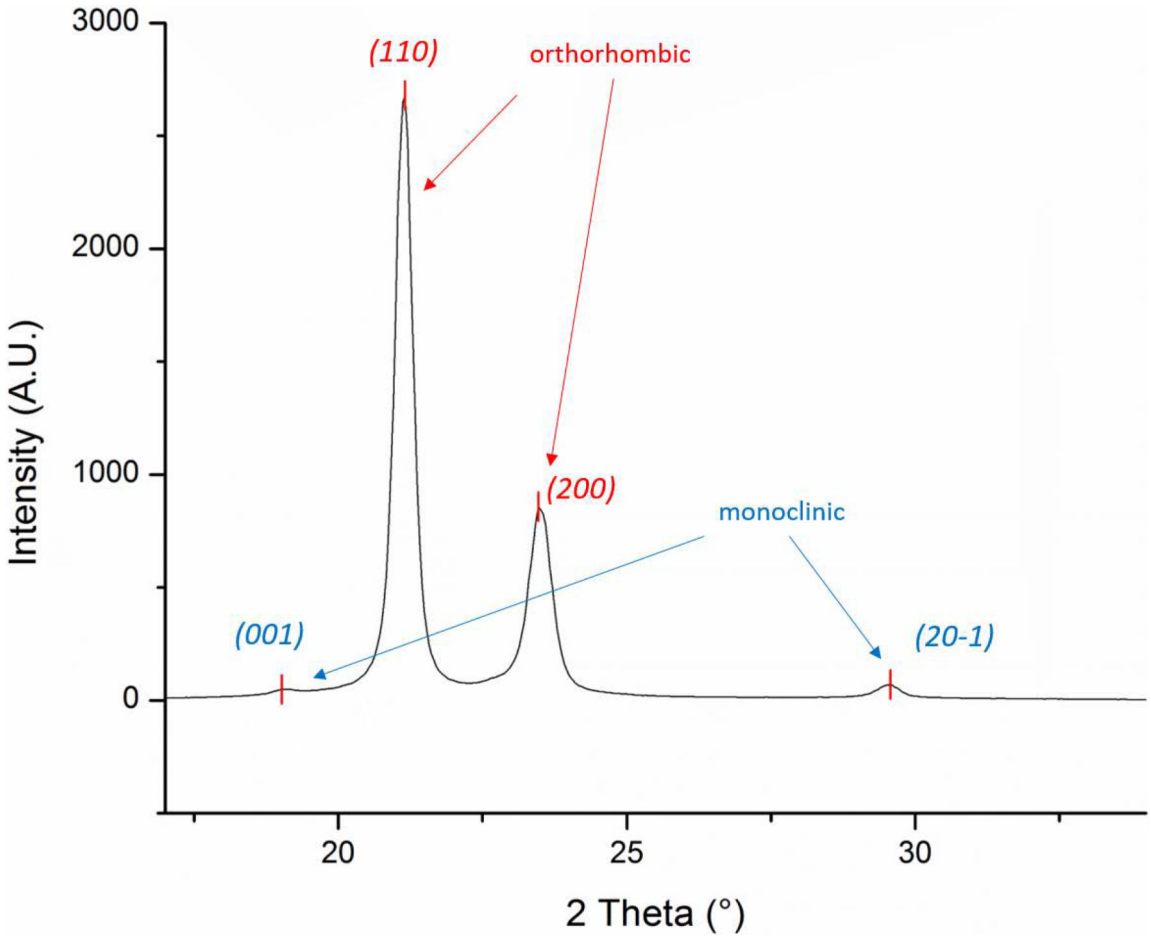

Fig. 8.

WAXS diffractograms of UHMMPE fibers extracted from new body armor panels. The diffraction was measured on a bundle of fibers placed horizontally, with their axis perpendicularly to the X-ray beam, at approximately 25° C. The intensity peaks for the orthorhombic and monoclinic crystal phases are shown.

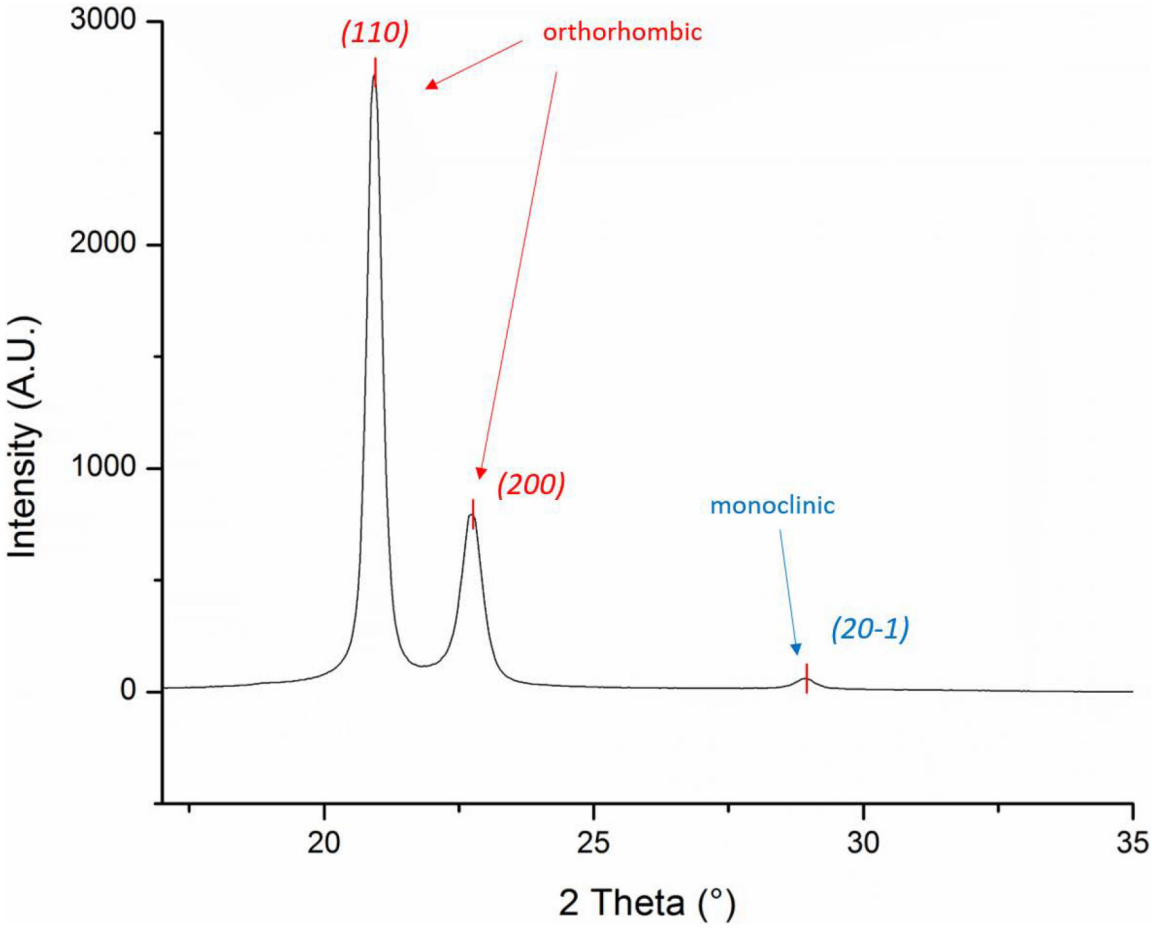

Fig. 9.

WAXS diffractograms of UHMMPE fibers extracted from new body armor panels. The diffraction was measured on a bundle of fibers placed horizontally, with their axis perpendicularly to the X-ray beam, at approximately 140 °C. The intensity peaks for the orthorhombic and monoclinic crystal phases are shown.

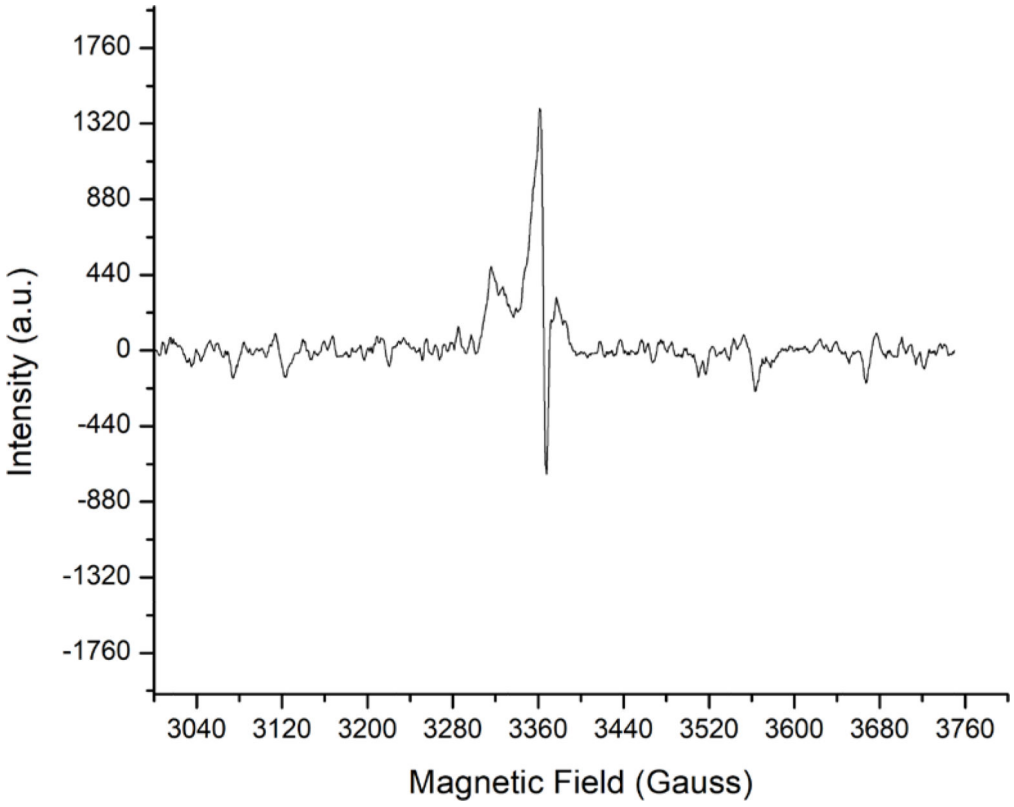

Fig. 10.

Electron Paramagnetic Resonance (EPR) of a kink banded UHMMPE after one year of discontinuing ageing.

Table 1

Changes in oxidation index (OI) of UHMMPE fibers upon conditioning. The data represented are mean ± S.E.M. (n ≥ 3).

	New Fibers	Normal – Folding	Kink Band – Folding	NIJ Conditioned Fibers
O.I. ($A1713cm^{-1}/A1471cm^{-1}$)	0.0127 ± 0.0016	0.0224 ± 0.0063	0.0497 ± 0.00582	0.0719 ± 0.0059

Table 2

Summary of melting points, heat of fusion, and crystallinity for UHMMPE fibers extracted from new and NIJ conditioned body armor. Note that the melting peaks and the total % crystallinity (X_C) do not change significantly.

UHMMPE Fibers Conditioning	Monoclinic T_{m1} (°C)	Orthorhombic T_{m2} (°C)	Mesophase T_{m3} (°C)	Hexagonal T_{m4} (°C)	ΔH_f J/g	X_c %
New	136	147	153	159	260.4	**90**
80 °C, 65% relative humidity, 5 rpm, 14 days	136	147	154	158	254	**87.8**

Table 3

Summary of the crystal phase percentages for UHMMPE fibers extracted from new and NIJ conditioned body armor. Calculations were done by fitting and integrating the DSC endotherms using commercial software.

UHMMPE Fibers Conditioning	Crystal Phase Percentages			
	Monoclinic	Orthorhombic	Mesophase	Hexagonal
New	1.8%	76.7%	20.3%	1.2%
80 °C, 65% relative humidity, 5 rpm, 14 days	1.9%	70.4%	26.1%	1.6%